Following a chemical reaction using high-harmonic spectroscopy

Worner, H. J.; Bertrand, J. B.; Kartashov, D. V.; Corkum, P. B.; Villeneuve, D. M.

Publisher's version / Version de l'éditeur:
https://doi.org/10.1038/nature09185
Nature, 466, 7306, pp. 604-607, 2010-07-01

Vol 466|29 July 2010|doi:10.1038/nature09185

LETTERS

Following a chemical reaction using high-harmonic interferometry

H. J. Wörner[1], J. B. Bertrand[1], D. V. Kartashov[1,2], P. B. Corkum[1] & D. M. Villeneuve[1]

The study of chemical reactions on the molecular (femtosecond) timescale typically uses pump laser pulses to excite molecules and subsequent probe pulses to interrogate them. The ultrashort pump pulse can excite only a small fraction of molecules, and the probe wavelength must be carefully chosen to discriminate between excited and unexcited molecules. The past decade has seen the emergence of new methods that are also aimed at imaging chemical reactions as they occur, based on X-ray diffraction[1], electron diffraction[2] or laser-induced recollision[3,4]—with spectral selection not available for any of these new methods. Here we show that in the case of high-harmonic spectroscopy based on recollision, this apparent limitation becomes a major advantage owing to the coherent nature of the attosecond high-harmonic pulse generation. The coherence allows the unexcited molecules to act as local oscillators against which the dynamics are observed, so a transient grating technique[5,6] can be used to reconstruct the amplitude and phase of emission from the excited molecules. We then extract structural information from the amplitude, which encodes the internuclear separation, by quantum interference at short times and by scattering of the recollision electron at longer times. The phase records the attosecond dynamics of the electrons, giving access to the evolving ionization potentials and the electronic structure of the transient molecule. In our experiment, we are able to document a temporal shift of the high-harmonic field of less than an attosecond (1 as = 10^{-18} s) between the stretched and compressed geometry of weakly vibrationally excited Br_2 in the electronic ground state. The ability to probe structural and electronic features, combined with high time resolution, make high-harmonic spectroscopy ideally suited to measuring coupled electronic and nuclear dynamics occurring in photochemical reactions and to characterizing the electronic structure of transition states.

To image a molecule with an intense femtosecond laser field ($\sim 10^{14}$ W cm^{-2}), we extract an electron wave packet from one of the valence orbitals and drive it back to interfere with the remaining bound electronic state. If the electron recombines, it emits extreme-ultraviolet (XUV) radiation in a train of attosecond pulses, a process known as high-harmonic generation (HHG). All molecules in the sample radiate coherently in a phase-matched process. HHG can image a molecular orbital[3] and probe rotational[7,8] and vibrational dynamics[9,10] in the electronic ground state. We demonstrate how HHG can also be applied to observe a chemical reaction in real time[11].

Molecular bromine (Br_2) serves as our exemplary molecule. Excitation at 400 nm transfers population from the X $^1\Sigma_g^+$ ground state to the repulsive C $^1\Pi_{1u}$ state in which it dissociates (Fig. 1a). Dissociation is essentially adiabatic, resulting in two bromine atoms in the $^2P_{3/2}$, $|m_J| = 1/2$ state[12]. High-harmonic generation from a coherent superposition of two electronic states can proceed by ionizing from and recombining to the same or the other electronic state (Supplementary Information section 1). All emitted fields are phase-locked to the generating field and interfere with each other, as illustrated in Fig. 1b. Once the overlap of the excited and ground-state

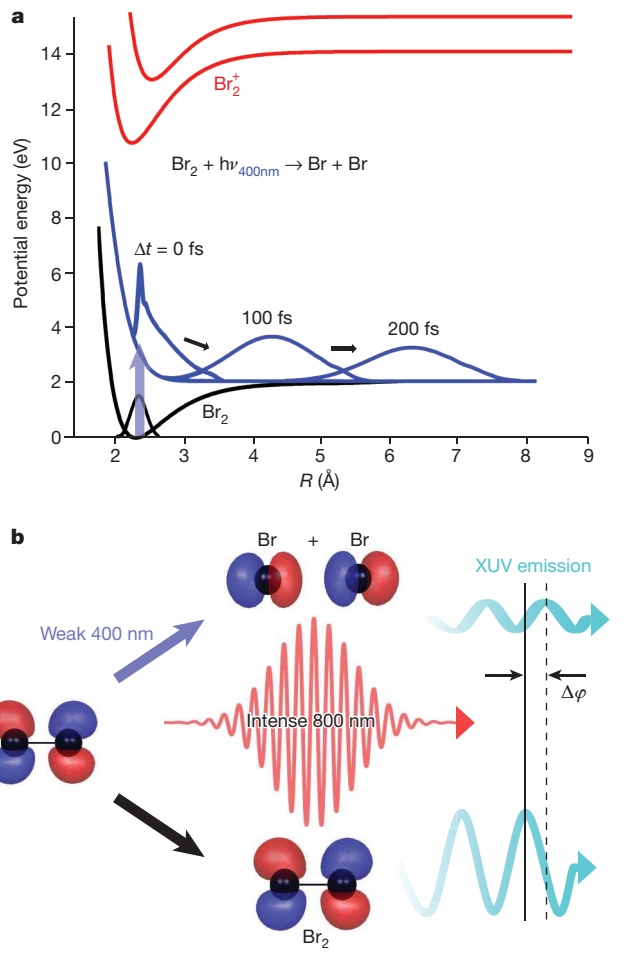

Figure 1 | High-harmonic interferometry of dissociating Br_2. **a**, Potential energy curves of the ground and excited (C $^1\Pi_{1u}$) state of Br_2 (black and blue lines, respectively) and the lowest electronic states of Br_2^+ (red lines) as a function of the internuclear separation, *R*. Also shown (thicker lines) are the ground-state nuclear wavefunction (black) and the calculated excited-state wave packet (blue) at selected delays Δ*t* following a 40-fs excitation pulse centred at 400 nm. **b**, Starting from the electronic ground state of Br_2, a small fraction of the sample is excited and undergoes dissociation. An intense 30-fs 800-nm pulse (red) probes the dissociation dynamics at variable delays after excitation. The two electronic states, represented by their most weakly bound orbital, emit high harmonics (turquoise) that differ in amplitude and in phase (Δφ).

[1]Joint Laboratory for Attosecond Science, National Research Council of Canada and University of Ottawa, 100 Sussex Drive, Ottawa, Ontario K1A 0R6, Canada. [2]Institut für Photonik, Technische Universität Wien, Gusshausstr. 25-29, 1040 Wien, Austria.

vibrational wave packets is lost, however, the coherent superposition can no longer be distinguished from a mixed sample of distinct ground-state and excited-state molecules. Only harmonics created by ionizing and recombining to the same state are possible.

We form a sinusoidal grating of excited molecules using two pump beams that cross in the medium, as shown in Fig. 2a. Horizontal planes of excited molecules alternate with planes of unexcited molecules. We generate high harmonics from this grating with a delayed 800-nm laser pulse (probe). The experiment is described in Methods. Figure 2b and c shows the yields of harmonics 13 to 21 in both the zero-order (Fig. 2b) and the first-order diffraction (Fig. 2c). The intensity of the zero-order diffraction decreases in all harmonic orders following excitation and subsequently increases to a level that depends on the harmonic order. By contrast, the first-order diffraction signal (not present at negative times) increases, reaching its asymptotic value about 300 fs after the excitation pulse. The zero time-delay and a cross-correlation time of 50 fs is monitored through the appearance of even-order harmonics (Supplementary Information section 6).

From zero- and first-order diffraction, we uniquely extract the harmonic amplitude d_e/d_g and phase $|\varphi_e - \varphi_g|$ of the excited state relative to the ground state. (Here $d_{e,g}$ and $\varphi_{e,g}$ are respectively the harmonic amplitudes and phases of the ground (g) and excited (e) states, see Supplementary Information section 2). We show the experimentally determined values in Fig. 3, for pump and probe polarizations parallel (Fig. 3a) or perpendicular (Fig. 3b).

The different time evolution of the amplitude and the phase is striking. Whereas the phase reaches its asymptotic value after ~150 fs, the amplitude takes more than 300 fs. It is also notable that the temporal variation of the amplitude changes with the relative polarization of the excitation and harmonic generation pulses (Fig. 3a and b). In contrast, although the time-dependent phase is different for the different polarizations, it reaches the same asymptotic value at the same time delay. We will first concentrate on the phase, then discuss the amplitude.

There are two main contributions to the phase of high-harmonic radiation (Supplementary Information, section 3). First, the electron and the ion accumulate a relative phase between the time of ionization and the time of recombination. The phase shift between the same harmonic order q being emitted by two electronic states differing in ionization potential by ΔI_p can be expressed as $\Delta\varphi_q \approx \Delta I_p \bar{\tau}_q$ (ref 13), where $\bar{\tau}_q$ is the average transit time of the electron in the continuum.

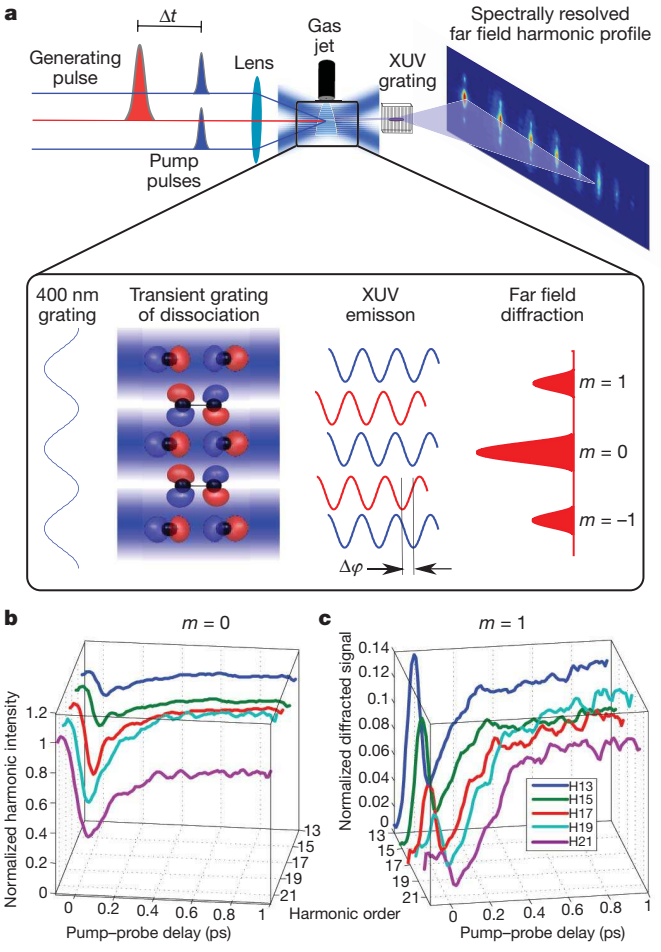

Figure 2 | High-harmonic transient grating spectroscopy. a, Two synchronized excitation pulses (400 nm) set up a transient grating of excitation in the molecular beam. A delayed 800-nm pulse generates high harmonics from the excited sample. The periodic modulation of the high-harmonic amplitude and phase in the near field (in the laser focus) results, in the far field (at the detector), in additional first-order diffraction ($m = 1$) signal. **b**, **c**, Evolution of the normalized intensities of harmonics 13 to 21 for parallel pump and probe polarizations in the zeroth order (**b**) and the first-order diffraction side band (**c**) with pump–probe delay. All signals have been normalized to the signal in the zeroth order at negative time delays, corresponding to molecules in the ground electronic state only.

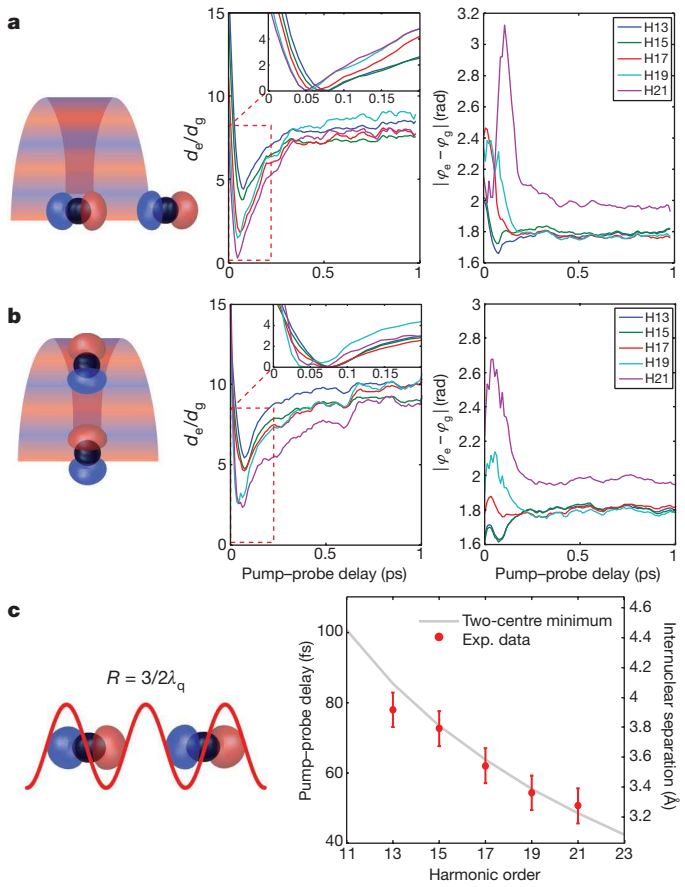

Figure 3 | Reconstruction of high-harmonic phases and amplitudes. **a**, **b**, Reconstructed amplitudes (middle) and phases (right) of the excited state relative to the ground state for parallel (**a**) and perpendicular (**b**) polarizations of the 400-nm excitation pulse relative to the 800-nm generating pulse. As the C ← X transition in Br_2 is perpendicular, the tunnel-ionized electron wave packet will follow a recolliding trajectory mostly perpendicular to the disk of excited molecules in **a** and parallel to it in **b**, as shown in the left column. In the insets of **a** and **b** (middle), the curves have been shifted vertically to show that the minimum occurs at different delays for different harmonic orders. **c**, Measured internuclear separation (R) as determined by the two-centre interference condition (illustrated on the left) of the dissociating molecule for each harmonic order q (error bars, s.d.). λ_q represents the de Broglie wavelength of the electron.

Second, when the electron recombines, the dipolar transition matrix element imposes an amplitude and a phase on the radiation[14,15]. The first contribution depends on the electron trajectory (determined by the laser parameters) and the ionization potential. The second contribution characterizes the electronic structure of the molecule. It depends on the emitted photon energy and the angle of recombination in the molecular frame[3].

The time evolution of the reconstructed phase in Fig. 3 can be split into two regions: the first 150 fs, where the phase varies rapidly, and the subsequent flat region where the phase is independent of the relative polarizations. The rapidly varying phase reflects the fast variation of the ionization potentials with delay. The strong dependence of the phase on the relative polarizations (Fig. 3a versus Fig. 3b) shows that the phase also traces the evolution of the electronic structure of the molecule as it dissociates. This variation occurs because the electronic structure of the bound state to which the electron recombines changes significantly. At asymptotic delays we measure Br atoms relative to ground state molecules. The phase shift is independent of the direction of recombination, because Br_2 dissociates into atoms in the $|m_j| = 1/2$ magnetic sub-level[12]. The phase shift is 1.8 rad for the thirteenth harmonic (H13). Using the relation $\Delta\varphi_q \approx \Delta I_p \bar{\tau}_q$, with $\bar{\tau}_q$ from a classical trajectory calculation[16], we obtain $\Delta I_p = 1.3$ eV, in good agreement with the known ionization potentials of Br_2 and Br.

We now turn to the temporal evolution of the amplitudes. All harmonics go through a deep minimum at an early time (Fig. 3a and b, insets). The minimum, occurring between 51 ± 5 fs (H21) and 78 ± 5 fs (H13), measures the stretching of the orbital as the molecule dissociates. We obtain almost identical results in both polarizations because at early delays the ionization step selects molecules lying parallel to the laser field. When the electron recombines to the initial state, its de Broglie wavelength λ_q can destructively interfere with the initial state wavefunction (Fig. 3c). When the molecular orbital is an in-phase combination of two atomic orbitals, destructive interference occurs for internuclear separations $R = [(2n+1)/2]\lambda_q$ (where n is an integer; ref. 17). Using $n = 1$ and the relation $\Omega = k^2/2$ between the photon energy Ω and the electron momentum k, we translate the minimum of H21 to a bond length of 3.3 Å and that in H13 to 3.9 Å (Fig. 3c)—in good agreement with wave-packet calculations (Supplementary Information section 4). Thus, we trace the bond length as a function of time using quantum interference.

As the molecule dissociates, one might expect additional minima corresponding to destructive interference with $n > 1$. Instead, we observe a slow rise of the amplitudes. At delays larger than 150 fs, the four valence molecular orbitals of Br_2 formed from the $4p$ atomic orbitals of Br become nearly degenerate, masking quantum interference in ionization or recombination. Consequently, it is only the propagation of the electron in the laser field that is affected by the second atom. For perpendicularly polarized pump and probe beams, the interaction of the ionized electron with the neighbouring atom is maximized, because the electron trajectory between tunnelling and recollision lies in the plane of the disk of dissociating atoms. As we show in Supplementary Fig. 5, the slower recovery of the amplitude in Fig. 3b reflects this fact. This property of high-harmonic spectroscopy is analogous to XAFS (extended X-ray absorption fine structure), and may be useful to probe the chemical environment of a low-I_p species (for example, a molecule in a helium droplet).

Time-resolved photoelectron measurements of the dissociation of Br_2 have demonstrated how the binding energies shift as the atoms move apart. In refs 18, 19 and 20, the time delay for the appearance of an atomic-like photoelectron spectrum is in the range 40–85 fs. In high-harmonic spectroscopy, recollision is sensitive to the electronic structure of the molecule rather than to the binding energy of individual orbitals. The minima between 50 and 80 fs show that the electron recombines with a two-centre molecular wavefunction. The absence of such minima between 100 and 150 fs suggests that at longer delays the recombination occurs to a single centre. An analogous transition between two- and one-centre signatures has recently been observed in core–shell photoionization of a static molecule[21]. However, the recovery of the amplitudes in Fig. 3a shows that the atomic character of the electronic wavefunction is only fully established after 300 fs, significantly later than the photoelectron measurements suggest.

Before concluding, we show that spectral interferometry with high harmonics is a general technique. In every photochemistry experiment creating atomic fragments, there is a second static reference naturally present at long time delays. In our case, for time delays greater than ~300 fs, the medium consists of alternating planes of ground-state molecules and atomic fragments. Increasing the pump intensity to the level where the ground state depletion becomes significant, a vibrational wave-packet motion is clearly seen in the phase (Fig. 4)—but not in the amplitude (not shown)—of the highest harmonics (H19 and H21). The minimal observed modulation depth of the relative phase amounts to 0.02 rad for H19. Using the equation $\Delta\varphi_q \approx \Delta I_p \bar{\tau}_q$, we measure ΔI_p as varying by 0.01 eV between the inner and outer turning points of the vibrational motion. We note that the measured phase shift corresponds to a temporal shift of the harmonic field of 450 zeptoseconds ($1\ \text{zs} = 10^{-21}$ s). The sinusoidal variation of the phase with time indicates an essentially linear variation of ΔI_p with R, which shows that the potential curves of the neutral and the ion are shifted with respect to each other[22].

Clearly, there is a close connection between high-harmonic and photoelectron spectroscopy. Photoelectron spectroscopy identifies excited-state dynamics by changes in the photoelectron energy[18,20] or angular distribution[23,24], whereas high-harmonic spectroscopy makes the identification through the interference of the emitted radiation. This interference gives high-harmonic spectroscopy access to both the amplitude and the phase of the recombination dipole. The phase of an outgoing photoelectron wave packet, in contrast, is very difficult to measure[25,26]. Measuring high-harmonic phase will allow us to investigate attosecond dynamics induced by the laser field, electronic wave packets launched through ionization[15], and non-adiabatic electronic dynamics[27,28].

Looking forward, measuring the amplitude and phase of the transition moment relative to a fully characterized ground-state reference[3] will allow dynamic imaging of orbitals in a chemical reaction. Other applications in femtochemistry are possible, ranging from simple dissociation dynamics, to proton transfer, to non-adiabatic reaction

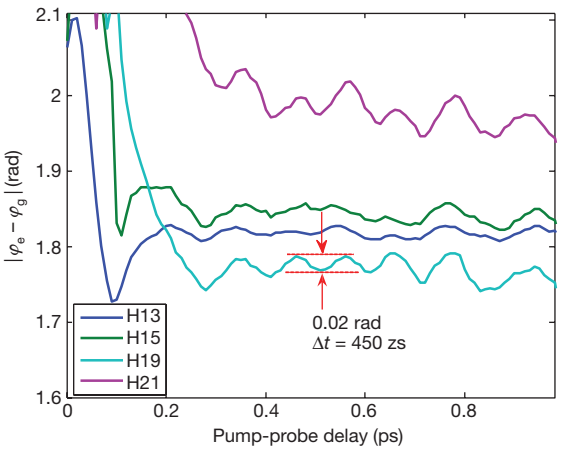

Figure 4 | Vibration-induced modulation of the high-harmonic phase. Reconstructed relative phases of harmonics 13 to 21 in an experiment similar to that shown in Fig. 3a but at higher intensity of the 400-nm excitation pulses. The fast transient in the first 200 fs measures the dissociation of the excited state. The subsequent modulation with a period of 100 fs measures the variation of the phase of the vibrating ground-state molecules relative to that of the atoms generated in the photo-dissociation process.

dynamics, to complex photochemical processes. For example, the change in electronic structure associated with the crossing of a conical intersection[29,30] will be mapped into the harmonic radiation. In all these cases, the sensitivity of high-harmonic spectroscopy to electronic structure will provide new insight.

METHODS SUMMARY

The experiment uses a chirped-pulse amplified titanium-sapphire femtosecond laser, a high-harmonic source chamber equipped with a pulsed valve and a XUV spectrometer. The laser beam, comprising 8-mJ pulses of 32-fs duration (full-width at half-maximum, FWHM) at 800 nm, is split into two parts of variable intensities using a half-wave plate and a polarizer. The major part is sent through a computer-controlled delay stage towards the high-harmonic chamber, while the minor part is sent through a type I BBO crystal of 100-μm thickness to generate 400-nm pulses. A 50:50 beamsplitter generates two equally intense 400-nm beams that are recombined on a dichroic mirror with the 800-nm beam. The two 400-nm beams and the 800-nm beam are all parallel to each other with a vertical offset of ± 0.75 cm, and focused into the chamber using an $f = 50$ cm spherical mirror. The focus of the 800-nm beam is placed 1 mm before the molecular jet to favour the short trajectories. Typical pulse energies amount to 1 mJ (800 nm) and 3 μJ (400 nm), resulting in respective intensities of 10^{14} W cm^{-2} (800 nm) and 10^{12} W cm^{-2} in the bright zones of the grating. High-order harmonics are generated in a supersonic expansion of Br_2 seeded in 2 bar of helium. The high harmonics generated by the 800-nm field are spectrally resolved using an aberration-corrected XUV grating and imaged by a micro-channel plate detector backed with a phosphorescent screen using a charge-coupled device camera. The images are transferred to a computer for analysis. The harmonic intensities are extracted by integrating the images spatially and spectrally. We have verified that the reconstructed phases and amplitudes shown in Fig. 3a and b are insensitive to the chirp of the 800-nm laser pulse.

Received 9 October 2009; accepted 20 May 2010.

1. Neutze, R., Wouts, R., van der Spoel, D., Weckert, E. & Hajdu, J. Potential for biomolecular imaging with femtosecond X-ray pulses. *Nature* **406,** 752–757 (2000).
2. Ihee, H. *et al.* Direct imaging of transient molecular structures with ultrafast diffraction. *Science* **291,** 458–462 (2001).
3. Itatani, J. *et al.* Tomographic imaging of molecular orbitals. *Nature* **432,** 867–871 (2004).
4. Meckel, M. *et al.* Laser-induced electron tunnelling and diffraction. *Science* **320,** 1478–1482 (2008).
5. Eichler, H. J., Gunter, P. & Pohl, D. W. *Laser-Induced Dynamic Gratings* Ch. 2–4 (Springer, 1986).
6. Mairesse, Y. *et al.* High-order harmonic transient grating spectroscopy in a molecular jet. *Phys. Rev. Lett.* **100,** 143903 (2008).
7. Itatani, J. *et al.* Controlling high harmonic generation with molecular wave packets. *Phys. Rev. Lett.* **94,** 123902 (2005).
8. Kanai, T., Minemoto, S. & Sakai, H. Quantum interference during high-order harmonic generation from aligned molecules. *Nature* **435,** 470–474 (2005).
9. Wagner, N. L. *et al.* Monitoring molecular dynamics using coherent electrons from high harmonic generation. *Proc. Natl Acad. Sci. USA* **103,** 13279–13285 (2006).
10. Li, W. *et al.* Time-resolved dynamics in N_2O_4 probed using high harmonic generation. *Science* **322,** 1207–1211 (2008).
11. Le, V. H., Le, A. T., Xie, R. H. & Lin, C. D. Theoretical analysis of dynamic chemical imaging using high-order harmonic generation. *Phys. Rev. A* **76,** 013414 (2007).
12. Rakitzis, T. P. & Kitsopoulos, T. N. Measurement of Cl and Br photofragment alignment using slice imaging. *J. Chem. Phys.* **116,** 9228–9231 (2002).
13. Kanai, T., Takahashi, E. J., Nabekawa, Y. & Midorikawa, K. Destructive interference during high harmonic generation in mixed gases. *Phys. Rev. Lett.* **98,** 153904 (2007).
14. Wörner, H. J., Niikura, H., Bertrand, J. B., Corkum, P. B. & Villeneuve, D. M. Observation of electronic structure minima in high-harmonic generation. *Phys. Rev. Lett.* **102,** 103901 (2009).
15. Smirnova, O. *et al.* High harmonic interferometry of multi-electron dynamics in molecules. *Nature* **460,** 972–977 (2009).
16. Corkum, P. B. Plasma perspective on strong-field multiphoton ionization. *Phys. Rev. Lett.* **71,** 1994–1997 (1993).
17. Lein, M., Hay, N., Velotta, R., Marangos, J. P. & Knight, P. L. Role of the intramolecular phase in high-harmonic generation. *Phys. Rev. Lett.* **88,** 183903 (2002).
18. Nugent-Glandorf, L. *et al.* Ultrafast time-resolved soft x-ray photoelectron spectroscopy of dissociating Br_2. *Phys. Rev. Lett.* **87,** 193002 (2001).
19. Nugent-Glandorf, L., Scheer, M., Samuels, D. A., Bierbaum, V. M. & Leone, S. R. Ultrafast photodissociation of Br_2: laser-generated high-harmonic soft x-ray probing of the transient photoelectron spectra and ionization cross sections. *J. Chem. Phys.* **117,** 6108–6116 (2002).
20. Wernet, P. *et al.* Real-time evolution of the valence electronic structure in a dissociating molecule. *Phys. Rev. Lett.* **103,** 013001 (2009).
21. Zimmermann, B. *et al.* Localization and loss of coherence in molecular double-slit experiments. *Nature Phys.* **4,** 649–655 (2008).
22. Huber, K. P. & Herzberg, G. *Molecular Spectra and Molecular Structure* Vol. IV, *Constants of Diatomic Molecules* 106–108 (Van Nostrand Reinhold, 1979).
23. Gessner, O. *et al.* Femtosecond multi-dimensional imaging of a molecular dissociation. *Science* **311,** 219–222 (2006).
24. Bisgaard, C. Z. *et al.* Time-resolved molecular frame dynamics of fixed-in-space CS_2 molecules. *Science* **323,** 1464–1468 (2009).
25. Wang, Z.-M. & Elliott, D. S. Determination of cross sections and continuum phases of rubidium through complete measurements of atomic multiphoton ionization. *Phys. Rev. Lett.* **84,** 3795–3798 (2000).
26. Park, H. & Zare, R. N. Molecular-orbital decomposition of the ionization continuum for a diatomic molecule by angle- and energy-resolved photoelectron spectroscopy. II. Ionization continuum of NO. *J. Chem. Phys.* **104,** 4568–4580 (1996).
27. Lezius, M. *et al.* Nonadiabatic multielectron dynamics in strong field molecular ionization. *Phys. Rev. Lett.* **86,** 51–54 (2001).
28. Litvinyuk, I. V. *et al.* Shakeup excitation during optical tunnel ionization. *Phys. Rev. Lett.* **94,** 033003 (2005).
29. Domcke, W., Yarkony, D. R. & Köppel, H. (eds) *Conical Intersections: Electronic Structure, Dynamics and Spectroscopy* (Adv. Ser. in Phys. Chem., Vol. 15, World Scientific, 2004).
30. Bucksbaum, P. H. The future of attosecond spectroscopy. *Science* **317,** 766–769 (2007).

Supplementary Information is linked to the online version of the paper at www.nature.com/nature.

Acknowledgements Funding from Canadian Institute for Photonic Innovation, NSERC and AFOSR is acknowledged. H.J.W. thanks the Swiss National Science Foundation (SNF) for a fellowship.

Author Contributions D.M.V. proposed the experiment. H.J.W. and J.B.B. performed the experiments. J.B.B. assembled the transient grating set-up. H.J.W. proposed and conducted the data analysis. J.B.B. and D.V.K. performed a preliminary experiment. D.M.V. and H.J.W. did the theoretical calculations. H.J.W., J.B.B, P.B.C. and D.M.V. interpreted the data and wrote the Letter.

Author Information Reprints and permissions information is available at www.nature.com/reprints. The authors declare no competing financial interests. Readers are welcome to comment on the online version of this article at www.nature.com/nature. Correspondence and requests for materials should be addressed to D.M.V. (david.villeneuve@nrc.ca).

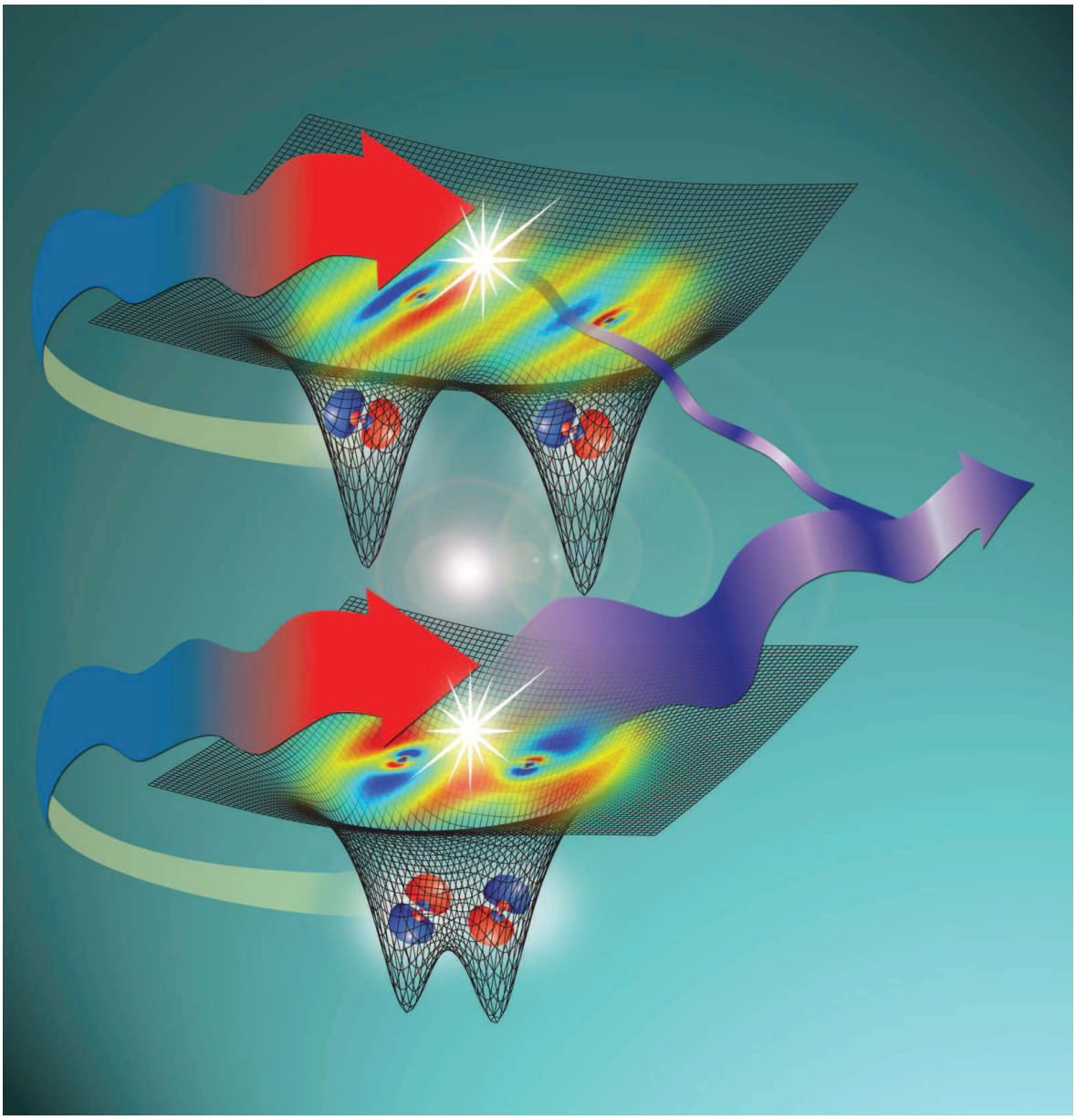

Fig. S1: **High-Harmonic Interferometry of a Chemical Reaction —** A weak femtosecond laser pulse excites a molecule from its ground state (on the bottom) to its excited state (on top) in which it dissociates. A strong femtosecond laser pulse removes an electron wave packet from the molecule through tunneling and accelerates it back to recollide with the parent molecule (red-blue arrows). The recollision results in emission of coherent soft-X-ray radiation (purple arrows). The figure illustrates schematically the molecular electrostatic potential and the orbital wave functions of the ground state (lower potential) and excited state (upper). We apply this method to repeatedly measure the structure of the molecule as it breaks in its excited electronic state. We exploit the static emission from the molecules in their ground state to measure, through coherent detection, both phase and amplitude of the light coming from a small number of excited molecules.

1 High-harmonic generation from a coherent superposition state

After photoexcitation, the molecule is in a coherent superposition of the ground state and an excited electronic state

$$\Psi(\vec{r},R) = c_g\Phi_g(\vec{r},R)\chi_g(R) + c_e\Phi_e(\vec{r},R)\chi_e(R), \tag{1}$$

where Φ_g and Φ_e are the electronic wave functions of the ground and excited electronic states, χ_g and χ_e are the vibrational wave functions in the two states and c_g and c_e are the wave function coefficients. The electronic wave functions depend on the electronic coordinates $\vec{r}$ and depend parametrically on the internuclear separation R. The vibrational wave functions depend only on the internuclear separation R.

Using the strong-field approximation[1], the high-harmonic emission from this coherent superposition can be expressed as[2]

$$\begin{aligned}
d_{\mathrm{HHG}}(t) = \; & -i \int_0^t dt' \int d\vec{k} E(t') \mathrm{e}^{-i/2\int_{t'}^{t} dt'' \left[\vec{k}+\vec{A}(t'')\right]^2} && \text{(2a)}\\
\times \; & \Big(|c_g|^2 \langle\chi_g|\chi_g\rangle d_g^*(\vec{k},t) d_g(\vec{k},t') \mathrm{e}^{-iIp_g(t-t')} \\
+ \; & |c_e|^2 \langle\chi_e|\chi_e\rangle d_e^*(\vec{k},t) d_e(\vec{k},t') \mathrm{e}^{-iIp_e(t-t')} && \text{(2b)}\\
+ \; & c_e^* c_g \langle\chi_e|\chi_g\rangle d_e^*(\vec{k},t) d_g(\vec{k},t') \mathrm{e}^{-i(Ip_e t - Ip_g t')} && \text{(2c)}\\
+ \; & c_g^* c_e \langle\chi_g|\chi_e\rangle d_g^*(\vec{k},t) d_e(\vec{k},t') \mathrm{e}^{-i(Ip_g t - Ip_e t')} \Big), && \text{(2d)}
\end{aligned}$$

where

$$d_i(\vec{k},t) = \langle \vec{k},t|\hat{r}_x|\Phi_i\rangle \tag{3}$$

and

$$\langle\vec{r}|\vec{k},t\rangle = (2\pi)^{-3/2} \mathrm{e}^{i[\vec{k}+\vec{A}(t)]\cdot\vec{r}}, \tag{4}$$

where $\vec{k}$ is the momentum of the electron and $\vec{A}$ is the vector potential of the laser field.

Four terms contribute to high-harmonic generation from a coherent superposition of two electronic states (see Eqs. (2)). Term (2a) represents high-harmonic emission by ionisation from and recombination to the ground electronic state and term (2b) represents the analogous process for the excited electronic state. Terms (2c) and (2d) represent events where ionisation takes place in the ground (excited) state and recombination leads to the excited (ground) state. The latter two terms are multiplied by the overlap of the nuclear wave packets in the two electronic states. The term $\langle\chi_e|\chi_g\rangle$ falls off very quickly for a dissociating molecule. When this term can be neglected, HHG emission is the same as for an incoherent mixture of molecules in Φ_g or Φ_e: only the first two terms in Eq. (2) play a role.

The high-harmonic generation pathways corresponding to ionization from one state and recombination to the other state are spectrally shifted from the odd harmonics. This has been shown in Refs.[3,4]. For our case, where the two states differ in electronic parity, the emitted photon energy Ω is equal to

$$\Omega = \Omega_{ge} + 2n\omega, \tag{5}$$

where Ω_{ge} is the energetic separation of the two electronic states at the moment of excitation. In the case of Br_2, this means that the coherent pathway is accompanied by the emission of even-order harmonics. In the experiment, even-order harmonics are also generated by the overlap of the 400 and 800 nm laser field (see Fig. S3), which shows no evidence of the coherent pathways.

2 High-harmonic emission from two electronic states and the transient grating

Assuming that the fraction of excited molecules is r (i.e. $|c_e|^2 = r$ and $|c_g|^2 = 1 - r$), that the amplitude and phase of harmonic emission are d_g and ϕ_g for the ground state and d_e and ϕ_e for the excited state, respectively, we introduce the relative amplitude $d_r = \frac{d_e}{d_g}$ and the relative phase $\Delta\phi = \phi_e - \phi_g$. The observed harmonic intensity for collinear excitation and high-harmonic generation pulses is:

$$\begin{aligned} I_{\text{total}}(r) &= |(1-r)d_g e^{i\phi_g} + r d_e e^{i\phi_e}|^2 \\ &= (1-r)^2 d_g^2 + r^2 d_e^2 + 2r(1-r) d_g d_e \cos(\Delta\phi) \\ &= d_g^2 \left(1 + 2r(d_r \cos(\Delta\phi) - 1) + r^2(d_r^2 - 2d_r \cos(\Delta\phi) + 1)\right). \end{aligned} \tag{6}$$

Normalization to the intensity from the unexcited sample (equal to d_g^2) provides

$$\frac{I(r)}{I(r=0)} = 1 + 2r\left(d_r \cos(\Delta\phi) - 1\right) + r^2\left(d_r^2 - 2d_r \cos(\Delta\phi) + 1\right). \tag{7}$$

In the transient grating geometry, the excited state amplitude is periodically modulated between 0 and $2r$ across the sample in the transverse direction with the spatial frequency k. The electric field of high harmonic emission from the ground state across a 1D-grating is

$$E_g(x) = d_g e^{i\phi_g}\left(1 - r(\cos(kx) + 1)\right) \tag{8}$$

and from the excited state

$$E_e(x) = d_e e^{i\phi_e} r(\cos(kx) + 1). \tag{9}$$

The signal in the far-field is the Fourier transform of this with the spatial frequency ξ

$$FT(E_g{+}E_e) = \left(d_g e^{i\phi_g}(1-r) + d_e e^{i\phi_e} r\right)\delta(\xi) + \frac{r}{2}\left(d_e e^{i\phi_e} - d_g e^{i\phi_g}\right)\left(\delta(\xi - \frac{k}{2\pi}) + \delta(\xi + \frac{k}{2\pi})\right). \tag{10}$$

The observed intensity distribution in the far-field is the power spectrum of Eq. (10) which means that the zeroth order has the intensity

$$\begin{aligned} I_{m=0} &= |d_g e^{i\phi_g}(1-r) + r d_e e^{i\phi_e}|^2 \\ &= d_g^2 |(1-r) + r d_r e^{i\Delta\phi}|^2 \\ &= d_g^2 \left(1 + 2r\left(d_r \cos(\Delta\phi) - 1\right) + r^2(d_r^2 - 2d_r\cos(\Delta\phi) + 1)\right) \end{aligned} \tag{11}$$

Normalizing to the zeroth order before excitation provides

$$I_{m=0,n} = \frac{I_{m=0}}{I_{m=0}(r=0)} = \left(1 + 2r\left(d_r\cos(\Delta\phi) - 1\right) + r^2(d_r^2 - 2d_r\cos(\Delta\phi) + 1)\right) \tag{12}$$

A single first order diffraction peak has the intensity

$$\begin{aligned} I_{m=1} &= |\frac{r}{2}(d_e e^{i\phi_e} - d_g e^{i\phi_g})|^2 \\ &= d_g^2 \frac{r^2}{4}(d_r^2 - 2d_r\cos(\Delta\phi) + 1), \end{aligned} \tag{13}$$

and the normalized signal

$$I_{m=1,n} = \frac{I_{m=1}}{I_{m=0}(r=0)} = \frac{r^2}{4}\left(d_r^2 - 2d_r\cos(\Delta\phi) + 1\right). \tag{14}$$

Therefore, using r from the calculations described in Section 4, one can extract

$$d_r\cos(\Delta\phi) = \frac{I_{m=0,n} - 4I_{m=1,n} - 1}{2r} + 1 \tag{15}$$

and

$$d_r^2 = \frac{4}{r^2} I_{m=1,n} + 2d_r\cos(\Delta\phi) - 1, \tag{16}$$

and because $d_r\cos(\Delta\phi)$ was determined above, one gets d_r and thus $|\Delta\phi|$.

The excited state fraction r varies from 0 to r_{max} during the excitation pulse. To reconstruct d_e/d_g and $|\phi_e - \phi_g|$ from the experimental data we use the error function $\mathrm{erf}(x)$ representing the integral of the Gaussian pulse envelope $G(t) = I_0\exp(-t^2/2\sigma^2)$

$$r(\Delta t) = r_{max}\frac{1 + \mathrm{erf}(\frac{\Delta t}{\sigma\sqrt{2}})}{2}, \tag{17}$$

where r_{max} is calculated by solving the time-dependent Schrödinger equation of a two state problem using the experimentally determined potential energy curves and transition dipole moments from Ref.[7].

3 Phase of high-harmonic radiation

In the strong-field approximation, the phase of a given harmonic q has three contributions: the classical action of the laser field on the electron along its trajectory (Volkov phase), the phase accumulated by the ion relative to the neutral while the electron is in the continuum (I_p phase) and the phase resulting from the emission time of the harmonic (emission phase). Mathematically, this can be expressed as:

$$\phi_q(t, t', \vec{p}) = \int_{t'}^{t} dt'' \left[\frac{(\vec{p} - \vec{A}(t''))^2}{2} + I_p \right] - \Omega t, \tag{18}$$

where $\Omega = q\omega$, q is the harmonic order, ω the fundamental frequency, t' the time of ionisation and t the time of emission.

Now, if two electronic states with I_{p1} and I_{p2} emit in the same laser field, their harmonic phase can be calculated according to Eq. (18). We restrict our analysis to the short electron trajectories. If $\Delta I_p = I_{p2} - I_{p1}$ is small compared to the emitted photon energy and because the total phase must be stationary, the difference in Volkov and emission phases cancels to first order in the transit time $\tau = t - t'$. Therefore the relative harmonic phase of the two electronic states is approximately given by[5,6]

$$\Delta\phi_q \approx \Delta I_p \bar{\tau}(q), \tag{19}$$

where $\bar{\tau}(q)$ is the average transit time for electrons originating from the two electronic states.

In the presence of a non-zero-range potential, an additional phase contribution comes from the ionisation and the recombination that will depend on the electronic state and the angle θ of the fundamental laser field with respect to the molecular axis. Thus, the total phase difference between the harmonics emitted by the two electronic states can be expressed as

$$\Delta\phi_q \approx \Delta I_p \bar{\tau}(q) + \Delta\phi_i(q, \theta) + \Delta\phi_r(q, \theta). \tag{20}$$

$\phi_i(q, \theta)$ is the phase of ionisation that will depend on the harmonic order and the angle θ, and $\phi_r(q, \theta)$ is the phase of the recombination dipole. The latter quantity carries information about the electronic structure of the molecule.

4 Wavepacket calculation of dissociation

We calculate the temporal evolution of the photodissociating nuclear wave packet on the repulsive C $^1\Pi_{1u}$ state of Br_2 by solving the time-dependent Schrödinger equation using the split-operator technique. The excited state potential curve is taken from Ref.[7]. The squared modulus of the calculated vibrational wave packet using an excitation pulse of 50 fs FWHM is shown in Fig. 1 of the main paper for delay times of 0, 100 and 200 fs. In addition, Fig. S2 shows the expectation value of the internuclear separation of the dissociating molecule.

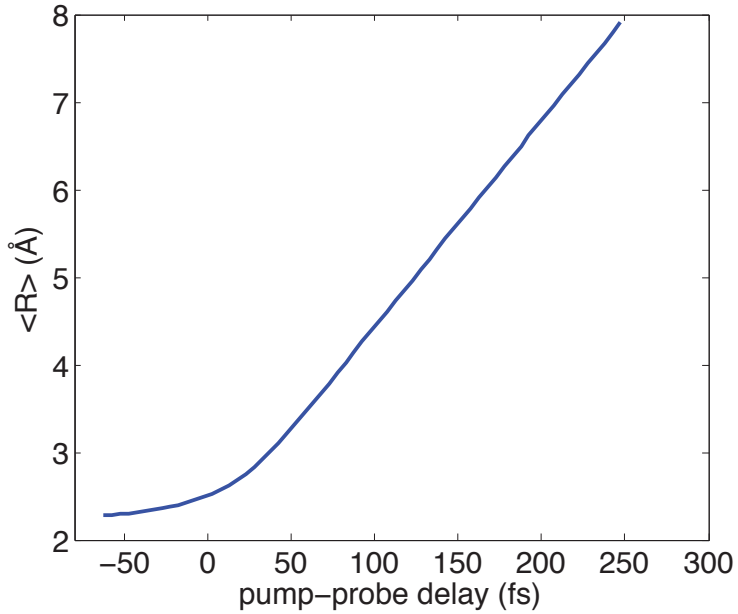

Fig. S2: Expectation value of the internuclear separation of Br_2 dissociating on the C $^1\Pi_{1u}$ state following photoexcitation by a 50 fs (FWHM) pulse centered at 400 nm.

5 Modeling of ground state vibrational wave packet

We theoretically model the ground state vibrations in Br_2 by solving the time-dependent Schrödinger equation of a two state model subject to a 400 nm pump pulse using the potential energy curves and transition dipoles given in Ref.[7]. Using a 400 nm pump pulse matching the experimental conditions of Fig. 4 of the main article, we find that the expectation value of the internuclear separation modulates with a period of 100 fs and an amplitude of $\pm$ 0.006 Å. We estimate the high-harmonic phase difference between the vibrating ground state molecule and the atomic fragments by calculating the expectation value of the phase given in Eq. (19) over the vibrational wave packet:

$$\phi_e - \phi_g = \arg\left(\int_0^\infty |\Psi_{vib}(R)|^2 \exp(i(I_p(Br) - I_p(Br_2, g)(R))\tau) dR\right). \quad (21)$$

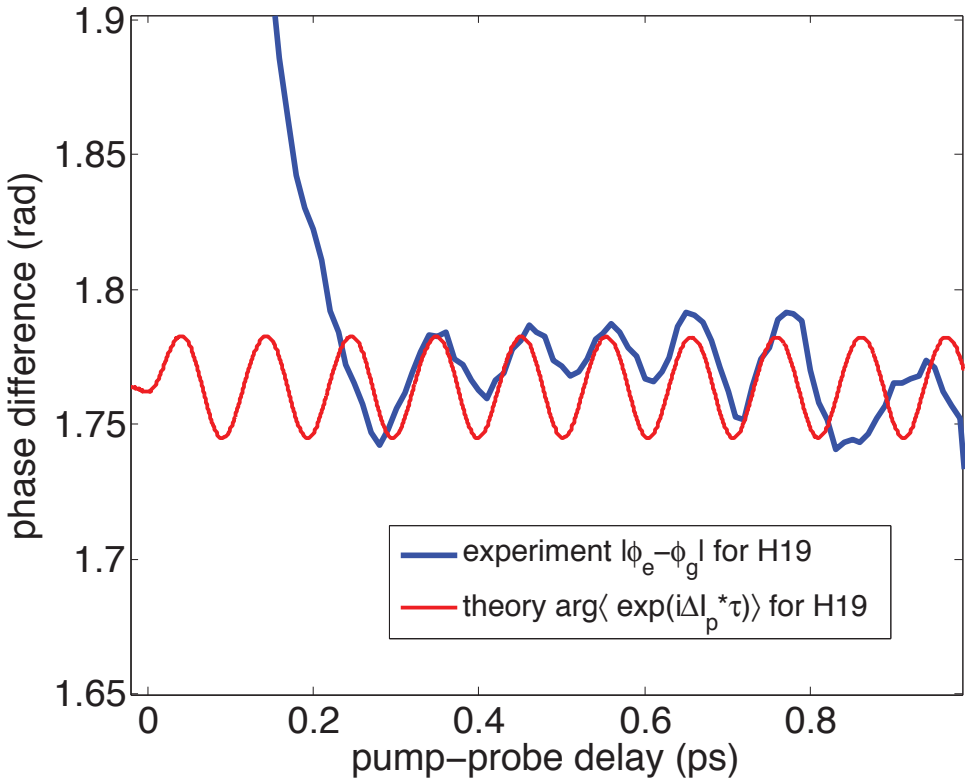

Fig. S3: Comparison of the reconstructed relative phase of H19 shown in Fig. 4 of the main article (blue line) with the theoretical value calculated as described in the above text (shifted vertically).

6 Additional experimental data

Fig. S4 illustrates the temporal resolution provided by our experiment. It shows the variation of the intensity of the zeroth order of H19 together with the variation of H20. The data is taken from the same experimental data set as Fig. 2 of the main article. The even harmonics are generated when the 800 nm and the 400 nm fields overlap because of the lost inversion symmetry of the electric fields. The appearance of even harmonics indicates the zero time delay and their width provides a high-order cross-correlation time of the two laser pulses. In Fig. S4 the FWHM of H20 amounts to 50 fs.

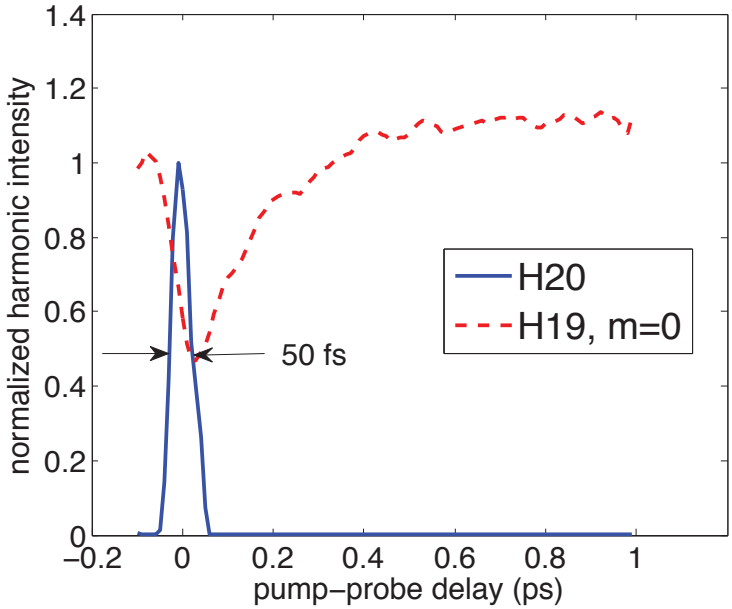

Fig. S4: Normalized intensities of the zeroth order of H19 (dashed red line) and the first order of H20 (full blue line) taken from the data set that was used to produce Fig.2 in the main article. The full-width-half-maximum of H20 amounts to 50 fs.

7 Analysis of high-harmonic amplitude dynamics

To quantify the time-evolution of the high-harmonic amplitudes shown in Fig. 3 of the main article, we have determined the delay at which the amplitude has recovered to half the asymptotic value and plot the result in Fig. S5. This delay is nearly independent of the harmonic order in the case of Fig. 3 (a) amounting to 170±10 fs, whereas in case of Fig. 3 (b) it increases linearly from 150±10 fs (H13) to 300±10 fs (H21) corresponding to internuclear separations increasing from 5.6 Å to 9.1 Å. The classical excursion amplitudes of the electron in the continuum increase from 2.6 Å to 6.6 Å over the same range of harmonics, as represented by the red line in Fig. S5, highlighting the direct relation between the extension of the electron trajectory and the internuclear separation.

We have thus shown that the high harmonic amplitude is highly sensitive to the presence of a neighboring atom up to very large distances.

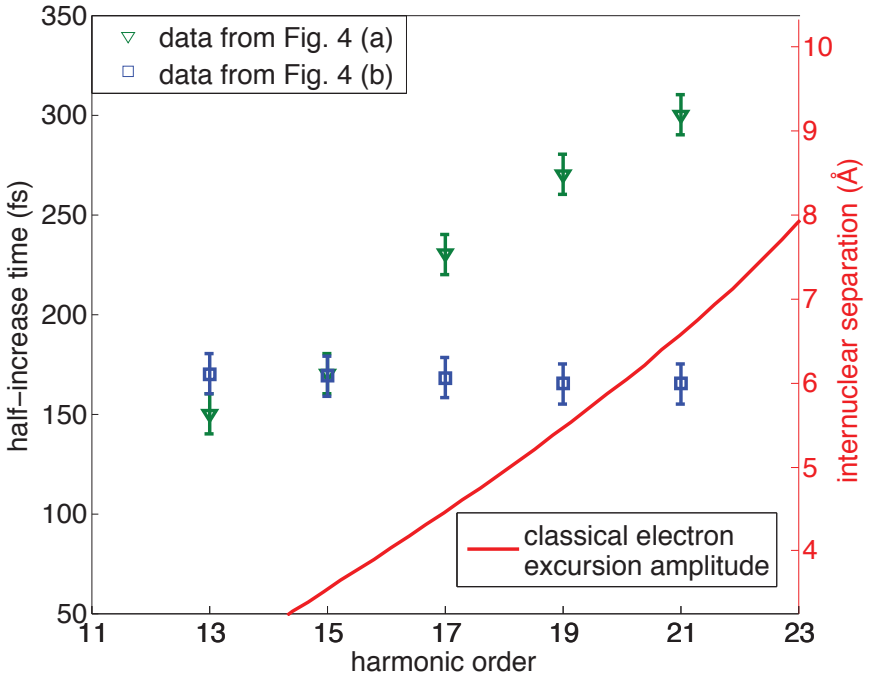

Fig. S5: Delays taken from Fig. 3 of the main article at which the amplitude d_e/d_g has recovered to half its asymptotic value. The right vertical axis represents the internuclear separation corresponding to the delay times indicated on the left vertical axis. The red line represents the extension of the classical electron trajectory corresponding to the emission of a given harmonic order.

It is interesting to note that there have been several single-electron, fixed-nuclei simulations suggesting that shorter wavelength high harmonics could be produced if dissociating molecules were used[8–11]. This experiment tests that hypothesis on a realistic molecular system for the first time. Our results suggest that the conditions to achieve an extended plateau using molecular dissociation will be hard to meet. As pointed out in Ref.[11], electron correlation suppresses these "transfer harmonics" in symmetrically dissociating homonuclear diatomic molecules.

1. Lewenstein, M., Balcou, P., Ivanov, M. Y., L'Huillier, A. & Corkum, P. Theory of high-harmonic generation by low-frequency laser fields. *Phys. Rev. A* **49**, 2117–2132 (1994).

2. Spanner, M. & Brumer, P. Probing electron transfer within alkali-metal halides via high-order harmonic generation. *Phys. Rev. A* **78**, 033840 (2008).

3. Watson, J. B., Sanpera, A., Chen, X. & Burnett, K. Harmonic generation from a coherent superposition of states. *Phys. Rev. A* **53**, R1962–R1965 (1996).

4. Milošević, D. B. Theoretical analysis of high-order harmonic generation from a coherent superposition of states. *J. Opt. Soc. Am. B* **23**, 308–317 (2006).

5. Kanai, T., Takahashi, E. J., Nabekawa, Y. & Midorikawa, K. Destructive interference during high-harmonic generation in mixed gases. *Phys. Rev. Lett.* **98**, 153904 (2007).

6. Smirnova, O., Patchkovskii, S., Mairesse, Y., Dudovich, N. & Ivanov, M. Y. Strong-field control and spectroscopy of attosecond electron-hole dynamics in molecules. *Proc. Nat. Ac. Sc. USA* **106**, 16556–16561 (2009), Supporting Information.

7. Le Roy, R. J., Macdonald, R. G. & Burns, G. Diatom potential curves and transition moment functions from continuum absorption coefficients: Br_2. *J. Chem. Phys.* **65**, 1485–1500 (1976).

8. Bandrauk, A. D., Chelkowski, S., Yu, H. & Constant, E. Enhanced harmonic generation in extended molecular systems by two-color excitation. *Phys. Rev. A* **56**, R2537–R2540 (1997).

9. Moreno, P., Plaja, L. & Roso, L. Ultrahigh harmonic generation from diatomic molecular ions in highly excited vibrational states. *Phys. Rev. A* **55**, R1593–R1596 (1997).

10. Kopold, R., Becker, W. & Kleber, M. Model calculations of high-harmonic generation in molecular ions. *Phys. Rev. A* **58**, 4022–4038 (1998).

11. Lein, M. Mechanisms of ultrahigh-order harmonic generation. *Phys. Rev. A* **72**, 053816 (2005).